Journal of Applied Mathematics and Physics, 2022, 10, 1495-1508
https://www.scirp.org/journal/jamp
ISSN Online: 2327-4379
ISSN Print: 2327-4352

Effect of the Relative Position with Gaussian Beam Center and Droplet Center on Optical Caustics

Yutong Hao

College of Science, University of Shanghai for Science and Technology, Shanghai, China
Email: 1720853339@qq.com

How to cite this paper: Hao, Y.T. (2022) Effect of the Relative Position with Gaussian Beam Center and Droplet Center on Optical Caustics. *Journal of Applied Mathematics and Physics*, **10**, 1495-1508.
https://doi.org/10.4236/jamp.2022.105105

Received: April 6, 2022
Accepted: May 13, 2022
Published: May 16, 2022

Abstract

In this paper, a vector ray-tracing model (VRT) is used to simulate the optical caustic structures associated with the secondary rainbow for an ellipsoidal droplet illuminated by a Gaussian beam. The optical caustics of drops with an equatorial radius a = 50 μm, 100 μm, 200 μm, and 500 μm are studied at the same drop/beam ratios (*i.e.* γ the ratio between the droplet equatorial radius and the Gaussian beam waist) using concentric illumination with a Gaussian beam, and the effect of droplet size on the optical caustics is analyzed. The curvature of the rainbow fringe and the evolution of the cusp caustics position, in this case, are obtained; the diameter range of droplet shape (ellipsoid) measured by Gaussian beam illumination is broadened. Based on this model, the effects of the relative positions $d = 0$, $0.5y_R$, and y_R on the optical caustics of the droplet when the center of the Gaussian beam deviates from the droplet center (the center of the Gaussian beam waist is on the same y-axis as the droplet center) are discussed. The optical caustics of the droplet when the center of the Gaussian beam is off the droplet center (the center of the Gaussian beam waist is on the z-axis with the droplet center) are also discussed. The effects of the relative positions of the center of the beam waist and the droplet center $d = 0$, $0.5y_R$, and y_R on the optical caustics are also discussed. A method of measuring droplet shape with Gaussian beam illumination is proposed when the beam waist center is coaxial with the droplet center.

Keywords

Vector Ray-Tracing Model, Optical Caustics, Gaussian Beam, Rainbow

1. Introduction

Roth [1] was the first to use CCD arrays to measure the position of the rainbow

angle to determine the droplet temperature and proposed a rainbow technique to measure the droplet particle size, refractive index, and temperature simultaneously by the rainbow angle of the primary rainbow. In 1984, Marston [2] experimentally probed hyperbolic umbilical fringes and the location of the cusps in the primary rainbow region of spherical droplet optical caustics. Subsequently, Nye [3] studied the aspect ratio of droplets producing hyperbolic umbilical fringe caustics, and the occurrence conditions of some characteristic optical caustics were predicted. Marston [4] found that the aspect ratio of droplets has a significant effect on the position of the cusps point with hyperbolic umbilical fringes, observed transverse cusp diffraction features [5], and further found mutation optics [6]. Dean [7] studied the expansion rate of the transverse cusp diffraction mutation. Nye [8] used mutation optics and geometric optics analysis to predict the ellipsoidal necessary to produce certain signature features of optical caustics, such as optical caustics in the equatorial plane, lip events, and E6 mutations. In addition, optical caustics by light scattering from circular droplets can also be observed under white illumination [9] [10]. A detailed study of the rainbow fringe structure in the secondary fringe and higher-order rainbow regions [11] [12] [13] and the optical caustics structure inside the liquid droplet [14] was also carried out. Jobe [15] analyzed the optical caustics scattering phenomenon in the primary rainbow region irradiated by a tilted Gaussian beam. Information such as droplet size, refractive index, and temperature can be determined based on the rainbow scattering of spherical droplets. And this method, known as the standard rainbow technique (SRT), can be used to characterize droplet information [16] [17] [18]. To measure the particle size distribution and the average temperature of a population of droplets in a spray, Van Beeck proposed global rainbow thermometry (GRT) [19] [20]. Both the SRT and GRT assume that droplets are spherical droplets. Wu developed a phase-rainbow refraction technique, which allows accurate measurement of droplet refractive indices and changes in tiny particle sizes to enable monitoring of droplet evaporation [21]. They also measured the droplet flow volumetric mixing ratio for several droplet mixtures using GRT [22]. Yu used generalized rainbow patterns to measure liquid droplet refractive index and particle size [18]. By obtaining the optical caustics structure of the scattering with an ellipsoidal droplet irradiated by a parallel beam, the curvature of the rainbow fringe and the position of the cusp point of the hyperbolic umbilical fringe were obtained. Gaussian beam illumination technology, the primary and higher-order characteristics of rainbow fringes were studied by Yu using the VRT model [23].

This article is organized as follows: The vector ray-tracing model for an oblate spheroidal drop with Gaussian beam illumination is described in Section 2. In Section 3, when a Gaussian beam is concentrically incident on an ellipsoidal droplet, the influence of the change of droplet size on the optical caustics is analyzed, and investigated its effect on the curvature of the rainbow fringes and the position of the cusp caustics. In Section 3, the influence of the incident ellipsoid droplet on the optical caustics when the Gaussian beam center is different from

the droplet center when the Gaussian beam incident position changes is described. The innovation of this paper is that by calculating the optical caustics of droplets with different particle sizes, it is proved that the model can be used to measure the aspect ratio of droplets with a wider range of particle sizes.

2. Vector Ray-Tracing Model for a Drop Illuminated with a Gaussian Beam

Assuming that the spherical center of the ellipsoid droplet is at the center of the Cartesian coordinate axis, label the spherical center as O_P. In this study, a Gaussian beam of *TEM00* is selected, whose waist radius is ω_0 and wavelength is λ, which propagates along the positive direction of the *x*-axis and is polarized along the *y*-direction. Let the center of the Gaussian beam be O_G coincident with the center of the sphere, as shown in Figure 1. The semi-axis lengths of the ellipsoid droplets are *a*, *b*, and *c*, respectively, and the refractive index is *m*. At this time, take the semi-major axis of the ellipsoid droplet $a = b$, $a > c$, $m = 1.33$.

At point A(*x*, *y*, *z*), under the first-order approximation, the phase of the incident Gaussian beam φ_i is given by

$$\varphi_i(x,y,z) = -k\left(y + \frac{x^2+z^2}{2R}\right) + \tan^{-1}\left(\frac{y}{y_R}\right) \tag{1}$$

where $k = 2\pi/\lambda$ is the wavenumber. The wavefront radius of curvature $R = y\left\{1+\left[y_R/y\right]^2\right\}$, Gaussian beams can be viewed as beam bundles within the framework of geometric optics. When a Gaussian beam encounters an ellipsoidal droplet, the direction vector of a ray of a Gaussian beam intercepting the ellipsoidal droplet is perpendicular to the wavefront of the local incident beam, which can be expressed as

$$\mathbf{L}_0 = L_x\vec{i} + L_y\vec{j} + L_z\vec{k} \tag{2}$$

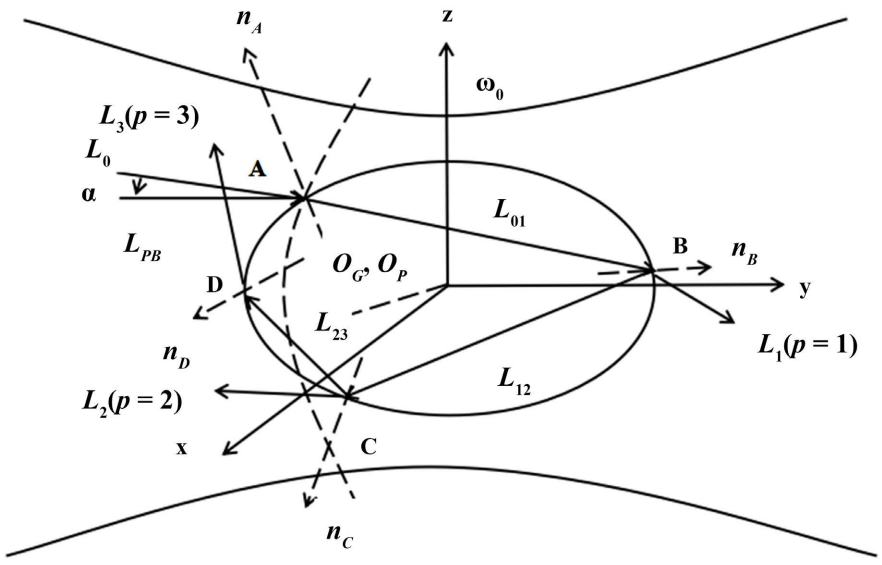

Figure 1. Vector ray tracing in an oblate droplet by a Gaussian beam.

$$L_x = -\frac{\partial \varphi_i}{\partial x} = \frac{2y_R xy}{\omega_0^2\left[y_R^2 + y^2\right]}$$

$$L_y = -\frac{\partial \varphi_i}{\partial z} = k + \frac{k\left(x^2 + z^2\right)\left[y_R^2 - y^2\right]}{\left[y^2 + y_R^2\right]^2} - \frac{y_R}{y_R^2 + y^2} \tag{3}$$

$$L_z = -\frac{\partial \varphi_i}{\partial z} = \frac{2y_R zy}{\omega_0^2\left[y_R^2 + y^2\right]}$$

Assuming that for a point A its coordinates are x_0, y_0 and z_0. By substituting x_0, y_0 and z_0 into Equation (2) and processing of the vector, one can obtain the incident unit vector at point A. The local beam radius ω is related to the beam waist radius ω_0 by $\omega = \omega_0\left\{1 + \left[y/y_R\right]^2\right\}^{1/2}$ and the Rayleigh length is $y_R = \pi\omega_0^2/\lambda$.

By using Snell's law, the refraction ray $\mathbf{L}_{01}$ can be obtained as

$$\mathbf{L}_{01} = \frac{1}{m}\left(\mathbf{L}_0 - \left(\mathbf{L}_0 \cdot \mathbf{n}_A\right)\mathbf{n}_A\right) - \sqrt{\left(1 - \frac{1}{m^2} + \frac{1}{m^2}\left(\mathbf{L}_0 \cdot \mathbf{n}_A\right)^2\right)}\mathbf{n}_A \tag{4}$$

where $\mathbf{n}_A$ is the surface normal at point A. The reflection ray at point B and C, the refraction ray at point D are given by

$$\mathbf{L}_{12} = \mathbf{L}_{01} - 2\left(\mathbf{L}_{01} \cdot \mathbf{n}_B\right)\mathbf{n}_B \tag{5}$$

$$\mathbf{L}_2 = m\left(\mathbf{L}_{12} - \left(\mathbf{L}_{12} \cdot \mathbf{n}_C\right)\mathbf{n}_C\right) + \sqrt{1 - m^2 + m^2\left(\mathbf{L}_{12} \cdot \mathbf{n}_C\right)^2}\mathbf{n}_C \tag{6}$$

$$\mathbf{L}_{23} = \mathbf{L}_{12} - 2\left(\mathbf{L}_{12} \cdot \mathbf{n}_C\right)\mathbf{n}_C \tag{7}$$

$$\mathbf{L}_3 = m\left[\mathbf{L}_{23} - \left(\mathbf{L}_{23} \cdot \mathbf{n}_D\right)\mathbf{n}_D\right] + \sqrt{1 - m^2 + m^2\left(\mathbf{L}_{23} \cdot \mathbf{n}_D\right)^2}\mathbf{n}_D \tag{8}$$

where $\mathbf{n}_B$, $\mathbf{n}_C$ and $\mathbf{n}_D$ are the normal vectors at points B, C and D respectively. The elevation and off-axis angles are defined in the same way as in reference [24].

3. Numerical Results

Figure 2 shows the optical caustics for a droplet with an equatorial radius a = 50 μm, 100 μm, 200 μm, and 500 μm; for a water drop with GB illumination and drop/beam ratios γ = 10. In Figure 2(a). In the horizontal direction, with a = 50 μm, the curvature of the rainbow fringes is more evident than for other fringes from θ = 126.92˚. The distance between the rainbow fringe and the hyperbolic umbilical fringe is closer than the optical caustics of the other droplet sizes, with an angular difference of 3.33˚. Figure 2(b) shows the optical caustics of the droplet by the Gaussian beam illumination when the a = 100 μm and γ = 10. Compared with the optical caustics of a = 50 μm, the rainbow fringe appears later, in this case, starting from θ = 128.46˚, and the cusp point appears at θ = 123.61˚. The angular difference between the horizontal direction of the rainbow fringe and the cusp point is 4.85˚. The distance between the rainbow fringes and the cusps with the a = 100 μm becomes farther than the a = 50 μm. Figure 2(c) shows the optical caustics by Gaussian beam illumination when the a = 200 μm. At this time, the rainbow fringe appears from θ = 128.93˚, while the cusp point

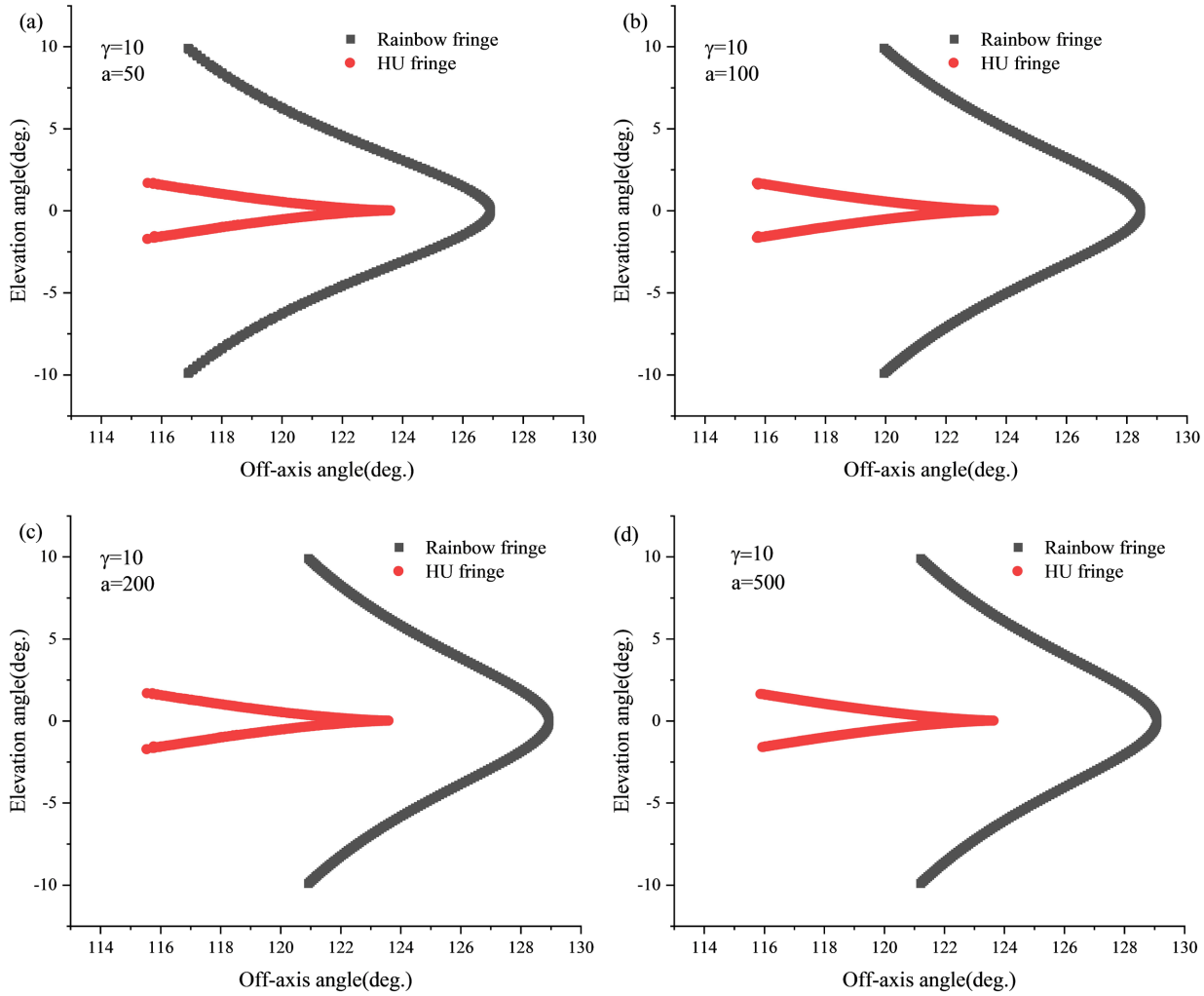

Figure 2. When $\gamma = 10$ and the aspect ratio of droplet is 1.37 (*i.e.*, $a/c = 1.37$), the optical caustics formed by the Gaussian beam incident on droplets of different sizes: (a) the equatorial radius $a = 50$ μm; (b) $a = 100$ μm; (c) $a = 500$ μm; (d) $a = 1000$ μm.

of the hyperbolic umbilical fringe appears at $\theta = 123.66^{\circ}$, and the angular difference between them is 5.27˚, which further increases the distance. When the droplet size increases to $a = 500$ μm, the rainbow fringe starts to appear from $\theta = 129.08^{\circ}$, the cusp point starts to appear from $\theta = 123.74^{\circ}$, and the angular difference between the two is 5.37˚. Compared with the droplets of the previous sizes, the angular difference gradually increases, and the distance gradually becomes more significant, as shown in **Figure 2(d)**.

For drop/beam ratio $\gamma = 10$, the optical caustics of droplet illuminated by Gaussian beam change with the droplet size. When the droplet size increases, the bending degree of rainbow fringes decreases, and the rainbow fringes moves to the right. The position of the cusp point gradually moved to the right, the angle difference between them gradually increased, and the distance gradually increased.

As can be seen from **Figure 3**, for drops with an equatorial radius $a = 50$ μm,

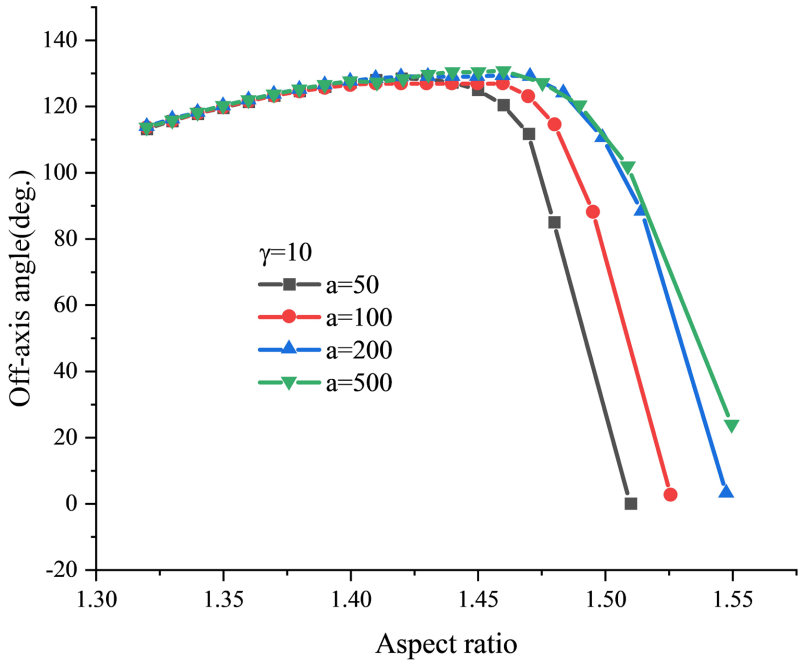

Figure 3. Location of cusp points for drop with different equatorial radius illuminated by GB.

the difference between the location of the cusp point and the other three particle sizes is the most obvious. When $a/c < 1.425$, the positions of the cusp point with the four droplet diameters almost coincide, they all increase gradually with the increase of the aspect ratio with the droplet. As the aspect ratio of the droplet continues to increase, the cusp point of the droplet with $a = 50$ μm gradually begins to separate from the cusp caustics of the droplet with $a/c = 1.47$, the angle of the cusp point is the largest. The difference between the droplet with an equatorial radius of $a = 50$ μm and the droplet with an equatorial radius of the other three is more obvious. When the aspect ratio of the droplet increases further, the angle of the cusp point of a droplet with four-particle sizes decreases gradually, and the difference between the position of the cusp point of a droplet with $a = 50$ μm, the other three droplet sizes increases further. At this time, when $a/c = 1.51872$ and $a = 100$ μm, the position of the cusp point with the droplet is gradually different from that of the droplet with $a = 200$ μm and 500 μm gradually decreases. As the droplet aspect ratio increases. The cusp point of the droplet with $a = 50$ μm disappears. The droplet cusp caustics angles of the other three sizes are increasing continuously. When the $a/c = 1.5269$, the cusp caustics of the droplet with $a = 100$ μm disappear. The droplets with $a = 500$ μm and 1000 μm are consistent and showed no significant difference. Cusp caustics in both cases were last seen at $a/c = 1.543$ and 1.54362, respectively.

Figure 4 shows that drop/beam ratios $\gamma = 10$, the curvature of rainbow fringe formed by Gaussian beam illumination ellipsoidal droplet changes with droplet size. When $a/c < 1.36$, the curvature of rainbow fringes of four droplet sizes is basically consistent, the curvature increases with the aspect ratio increase. When

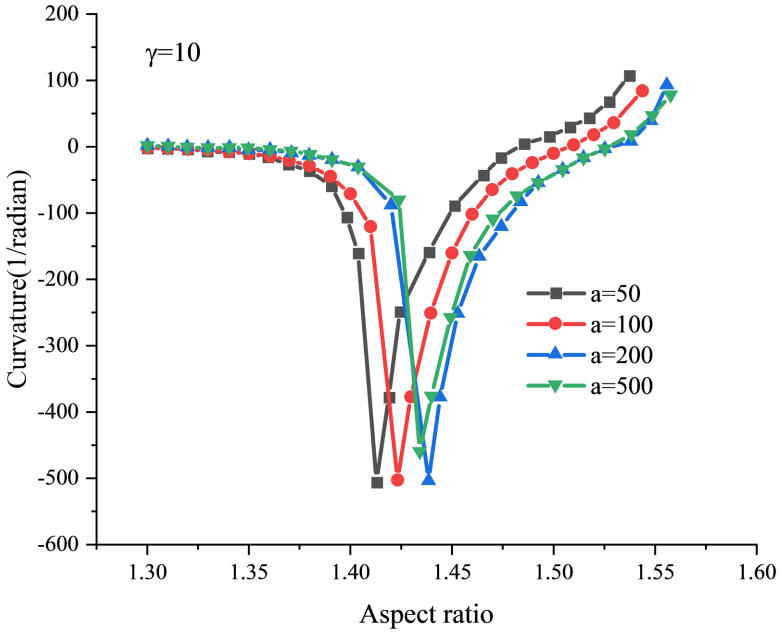

Figure 4. Curvatures of limiting rainbow fringes for drops with different equatorial radius illuminated by GB.

the aspect ratio continues to increase, the curvature of the rainbow fringe with the droplet with a = 50 μm decreases rapidly, which makes it gradually separate from the curvature trend with the other three particle sizes, and increases sharply when a/c = 1.372 because the deformation of the rainbow fringe is pronounced. When the aspect ratio continues to increase, the curvature of the other three rainbow fringes decreases slowly. When a/c = 1.4, the curvature of a = 100 μm rainbow fringes decreases rapidly, making it separate from the other two. When the aspect ratio of the droplet continues to increase, the curvature of the rainbow fringe with a = 50 μm and a = 100 μm droplet is still significantly different from the other two sizes. As the droplet aspect ratio increases, the curvature gradually decreases. At this time, when the aspect ratio is the same, the larger the particle size, the larger the curvature. When a/c = 1.415, the curvature of a = 50 μm droplet reaches a minimum and increases again with the ellipsoid degree. The curvature of a = 100 μm droplet reaches the minimum when a/c = 1.47 and increases again with the increase of ellipsoid. The a = 500 μm and 1000 μm reach the minimum value when a/c = 1.54 and continue to increase with the increase of aspect ratio. When the aspect ratio is the same, the curvature of the rainbow fringe decreases with the increase of droplet size.

This section shows, when γ is constant, optical caustics of droplets with different sizes irradiated on the y-axis with the center of a Gaussian beam, shown in Figure 5, which investigates the effect of the position of the Gaussian beam on the optical caustics with the droplets. In order to clearly show the effect of the relative position of the Gaussian beam and the droplet on the optical caustics, three special positions of d = 0, d = 0.5y_R, d = y_R are chosen. Where denotes the Rayleigh length, the aspect ratio of the droplet is 1.37.

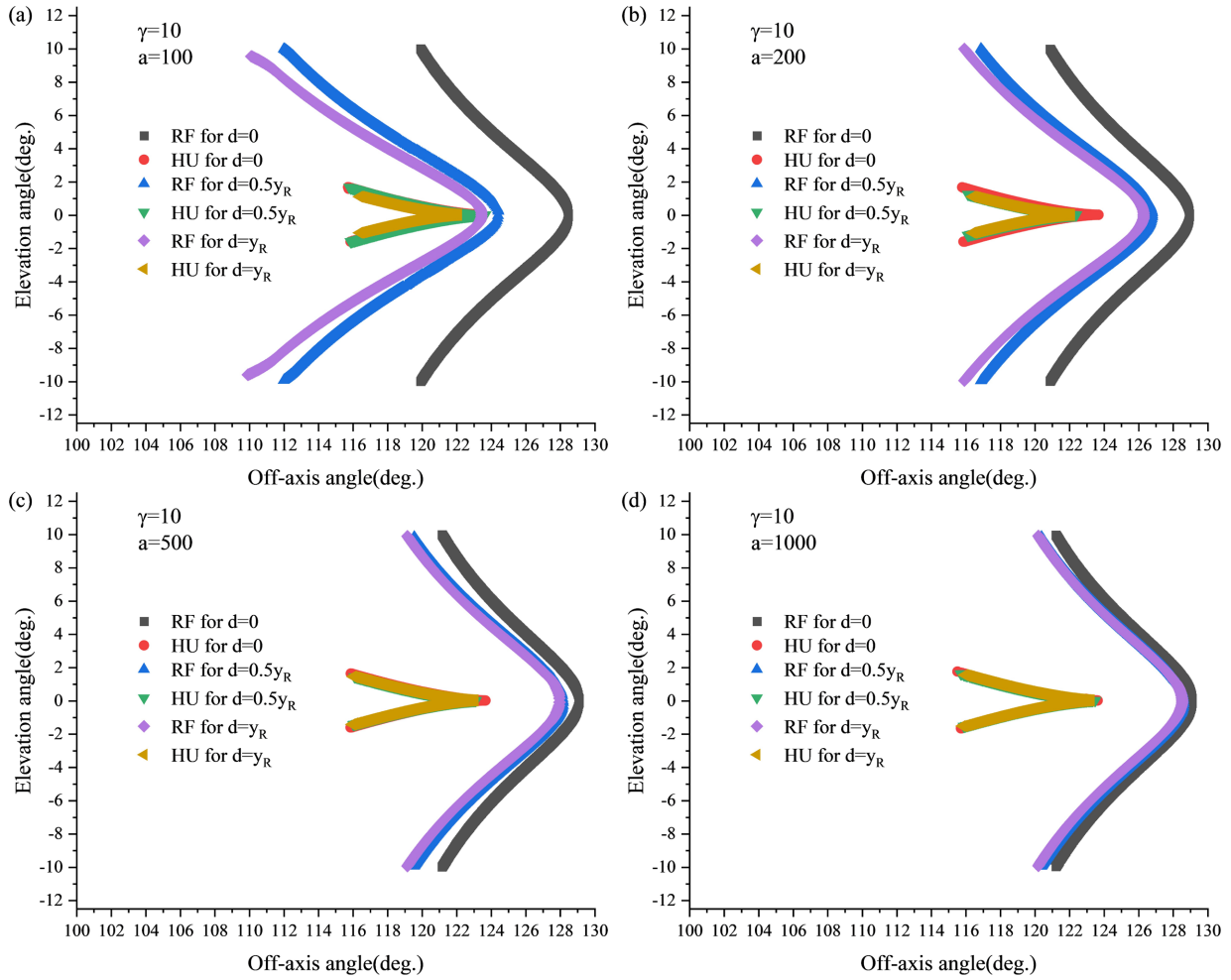

Figure 5. When $\gamma = 10$, the optical caustics formed by the Gaussian beam incident on the droplet from different positions: (a) the equatorial radius $a = 100$ μm; (b) $a = 200$ μm; (c) $a = 500$ μm; (d) $a = 1000$ μm. RF means rainbow fringes and HU means hyperbolic umbilical fringes.

Figure 5 shows the optical caustics of an ellipsoidal droplet incident from $d = 0$, $d = 0.5y_R$, and $d = y_R$ when drop/beam ratios $\gamma = 10$, where the droplet sizes are $a = 100$ μm, $a = 200$ μm, $a = 500$ μm, and $a = 1000$ μm, respectively.

From **Figure 5(a)**, it can be seen that when $a = 100$ μm, the angles of the rainbow fringe and hyperbolic umbilical fringe appear gradually increase as d increases. The angular difference between the three is obvious. When $d = 0$, the rainbow fringe appears at $\theta = 128.46^\circ$, while the hyperbolic umbilical fringe appears from $\theta = 124.53^\circ$, and the angle difference between the two is 3.93˚. When d increases to $0.5y_R$, the angle of optical caustics becomes significantly more prominent, with the rainbow fringe appearing at $\theta = 124.75^\circ$ and the hyperbolic umbilical fringe appears from $\theta = 121.9^\circ$, with an angular difference of 2.85˚ between the two. When d increases to y_R, the angle of optical caustics decreases further, the rainbow fringe appears at $\theta = 123.76^\circ$, and the hyperbolic umbilical fringe appears from $\theta = 121.63^\circ$, with an angular difference of 2.13˚. It can be found that when the droplet size is certain, the angle of optical caustics appears

more prominent as d increases. The angle difference between the rainbow fringe with the same d and the hyperbolic umbilical fringe gradually decreases, and the position gradually approaches. The angle differences between the rainbow fringes are 3.71˚ and 0.99˚, and the angle differences between the hyperbolic umbilical fringes are 2.63˚ and 0.27˚, both of which gradually decreases with the increase of d.

When a = 200 μm, as shown in Figure 5(b), it can be found that when d = 0, the first appearance of the rainbow fringe is θ = 128.94˚, while the first appearance of the hyperbolic umbilical fringe is θ = 124.23˚, and the angle difference between the two is 4.71˚. When d increases to $0.5y_R$, the rainbow fringe appears from θ = 127.21˚, while the hyperbolic umbilical fringe appears at θ = 122.74˚, with an angular difference of 4.47˚ between the two. When $d = y_R$, the rainbow fringe appears at θ = 126.16˚, and the hyperbolic umbilical fringe appears from θ = 122.32˚, with an angular difference of 3.84˚. The angular differences between the three rainbow fringes are 1.73˚ and 1.05˚, while the angular differences between the hyperbolic umbilical fringes are 1.49˚ and 0.42˚, respectively. As d gradually increases, the angular difference between the rainbow fringes and the hyperbolic umbilical fringes gradually decreases, representing that the positions are not moving away very fast.

Figure 5(c) shows the effect of Gaussian beam illumination position on optical caustics when a = 500 μm. When d = 0, the rainbow fringes appeared at θ = 129.35˚, and the hyperbolic umbilical fringes appeared at θ = 124.2˚, with an angle difference of 5.15˚. When $d = 0.5y_R$, rainbow fringes appeared at θ = 128.87˚, and hyperbolic umbilical fringes appeared at θ = 124˚, with an angle difference of 4.87˚. When d increases to y_R, rainbow fringes first appear at θ = 128.62˚, and hyperbolic umbilical fringes first appear at θ = 123.89˚, with an angle difference of 4.73˚. It can be found that the angle differences of the three rainbow fringes are 0.48˚ and 0.25˚, respectively, while the angle differences of the hyperbolic umbilical fringes are 0.2˚ and 0.11˚. With the increase of d, the angular deviation of optical caustics increases gradually, but the deviation decreases gradually.

The optical caustics with droplets with a = 1000 μm are shown in Figure 5(d). When d = 0, rainbow fringes appear at θ = 129.61˚, while hyperbolic umbilical fringes appear from θ = 123.98˚, and the difference between the angles is 5.63˚. When d increases to 0.5˚, rainbow fringes appear for the first time at θ = 129˚, and hyperbolic umbilical fringes appear for the first time at θ = 123.88˚, an angle difference of 5.12˚. Then, when $d = y_R$, the rainbow fringe appeared at θ = 128.94˚, the hyperbolic umbilical fringe appeared at θ = 123.85˚, the angle of 5.11˚ is different. The angle differences of the three rainbow fringes are 0.61˚ and 0.17˚, and the angle differences of the hyperbolic umbilical fringes are 0.1˚ and 0.09˚.

The above simulation results show that when γ = 10, the Gaussian beam incident the ellipsoidal droplet from three positions: d = 0, $d = 0.5y_R$, and $d = y_R$. There is a clear difference in the optical caustics. When d increases gradually, the angle at which the optical caustics appear increases, and the growth rate gradu-

ally slows down. As the droplet size increase, the angle difference of the optical caustics gradually decreases, and the optical caustics get closer and closer to the optical caustics of the parallel beam incident droplets. The reason for this has been discussed.

This paper also investigates the optical dispersion of the droplet when the center of the Gaussian beam is off the center of the droplet (the center of the Gaussian beam waist is on the same z-axis as the center of the droplet), the light is incident from $d = 0$, $d = 0.5y_R$, and $d = y_R$, respectively.

It can be seen from Figure 6(a) that when $a = 100$ μm, as d increases, the angles of the rainbow fringes and the hyperbolic umbilical fringes gradually increase, and the angle difference between the three is obvious. When $d = 0$, the rainbow fringes appear from the position of $\theta = 128.47^\circ$, and the elevation angle is 0.01˚. In contrast, the hyperbolic umbilical fringes appear from the position of $\theta = 123.69^\circ$, and the elevation angle is 0.05˚. When d increases to $0.5y_R$, the angle of optical caustics increases obviously. Rainbow fringes appear at $\theta = 128.55^\circ$

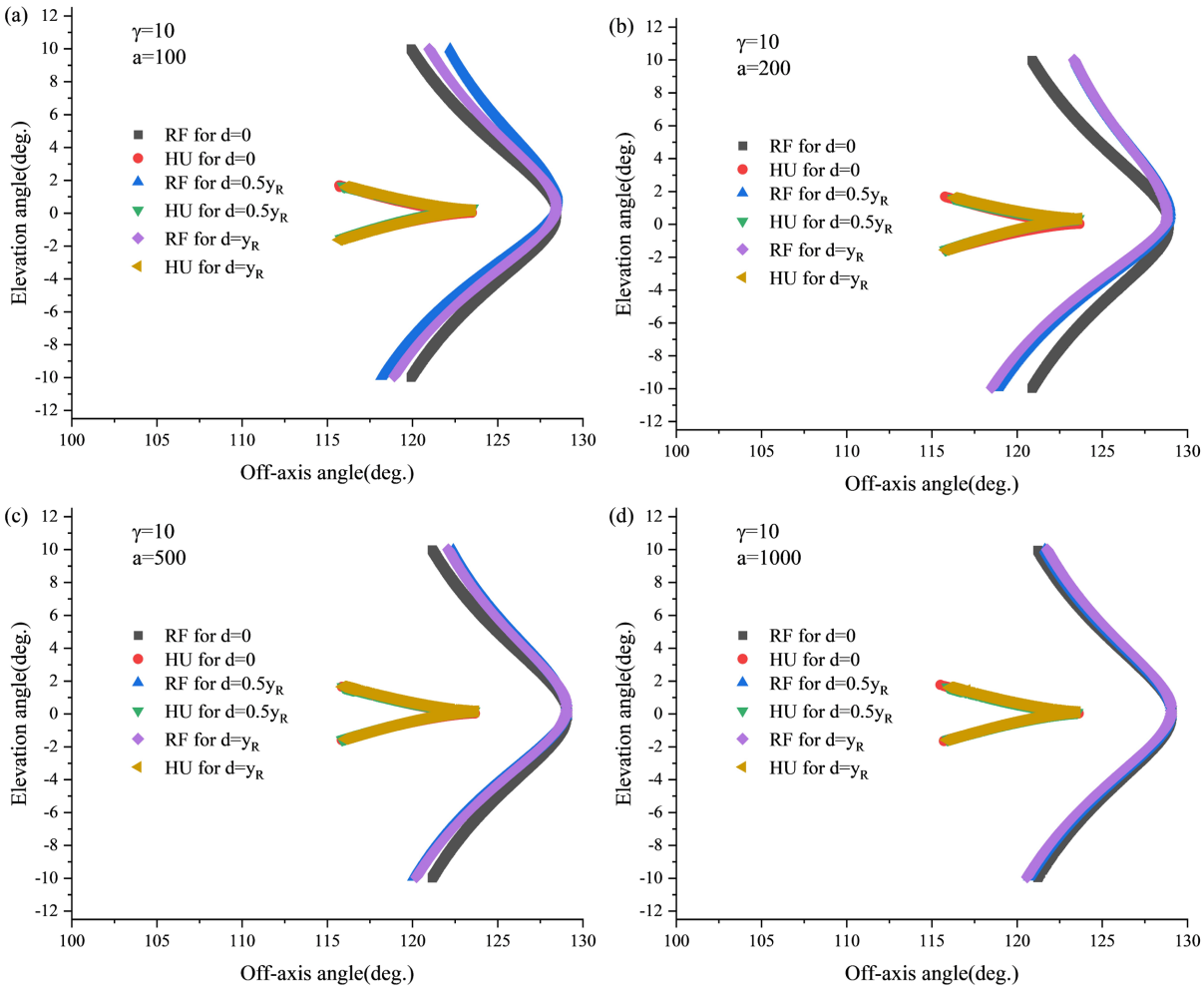

Figure 6. When $\gamma = 10$, the optical caustics formed by the Gaussian beam incident on the droplet from different positions: (a) the equatorial radius $a = 100$ μm; (b) $a = 200$ μm; (c) $a = 500$ μm; (d) $a = 1000$ μm. RF means rainbow fringes and HU means hyperbolic umbilical fringes.

with an elevation angle is 0.88˚, and hyperbolic umbilical fringes appear at θ = 123.61˚ with the elevation angle is 0.56˚. When d increases to y_R, the angle of the optical caustics becomes larger, and the rainbow fringes appear at θ = 128.49˚; the elevation angle is 1.12˚. The hyperbolic umbilical fringes appear at θ = 123.58˚, and the elevation angle is 0.62˚. It can be found that when the droplet with equatorial radius is constant, with the increase of d, the angle of the optical caustics elevation angle becomes larger and larger. The elevation angle difference between rainbow fringes is 0.87˚ and 0.24˚, and the elevation angle difference between hyperbolic umbilicus fringes is 0.51˚ and 0.06˚.

When a = 200 μm, as shown in Figure 6(b), it can be found that when d = 0, the angle at which the rainbow fringe first appears at θ = 128.94˚ and the elevation angle is 0.083˚, while the angle at which the hyperbolic umbilic fringe first appears at θ = 123.71˚ and the elevation angle is 0.06˚. When d increases to $0.5y_R$, rainbow fringes appear at θ = 129˚ with an elevation angle is 0.673˚, while hyperbolic umbilical fringes appear from θ = 123.79˚ with an elevation angle is 0.32˚. When $d = y_R$, the rainbow fringes appear at θ = 128.80˚ with the elevation angle is 0.733˚, and the hyperbolic umbilical fringes appear from θ = 123.68˚ with an elevation angle is 0.33˚. When the droplet size is constant, with the increase of d, the optical caustics elevation angle becomes larger and larger. The elevation angle difference between rainbow fringes is 0.59˚ and 0.06˚; the elevation angle difference between the hyperbolic umbilical fringes is 0.26˚ and 0.01˚. As d increases gradually, the angle difference between the rainbow fringes and the angle difference between the hyperbolic umbilical fringes gradually decrease, indicating that the position does not move away quickly.

Figure 6(c) shows the influence of the Gaussian beam irradiation position on the optical caustics when a = 500 μm. With d = 0, the rainbow fringes appear at the position of θ = 129.09˚, and the elevation angle is 0.13˚, the hyperbolic umbilical fringes appear from θ = 123.71˚, the elevation angle is 0.0043˚. When $d = 0.5y_R$, the rainbow fringes appear at θ = 129.05˚, the elevation angle is 0.49˚, and the hyperbolic umbilical fringes appear at θ = 123.69˚, and the elevation angle is 0.16˚. When d increases to y_R, the rainbow fringe first appears at θ = 129.095˚ with an elevation angle of 0.25˚, while the hyperbolic umbilical fringe first appears at θ = 123.76˚ with an elevation angle of 0.23˚. The elevation angle difference between rainbow fringes is 0.36˚ and 0.06˚, the elevation angle difference between hyperbolic umbilic fringes is 0.16˚ and 0.07˚. It can be found that with the increase of d, the angular deviation of the optical caustics also increases gradually, but the growth rate of the deviation gradually decreases.

The optical caustics when a = 1000 μm are shown in Figure 6(d). When d = 0, the rainbow fringe appears from θ = 129.094˚ with an elevation angle of 0.16˚, while the hyperbolic umbilical fringe appears at θ = 123.66˚ with an elevation angle of 0.00031˚. When $d = 0.5y_R$, the rainbow fringe first appeared at 129.095˚ with an elevation angle of 0.2˚, and the hyperbolic umbilical fringe first appeared at θ = 123.61˚ with an elevation angle of 0.05˚. Subsequently, when $d = y_R$, the rainbow fringe appears at θ = 129.094˚ with an elevation angle of 0.23˚, and the

hyperbolic umbilical fringe appears from $\theta = 123.58^{\circ}$ with an elevation angle of 0.07˚. When the droplet with equatorial radius is certain, the angle of the elevation angle of optical caustics becomes larger and larger as d increases. The elevation angle differences between the rainbow fringes are 0.04˚ and 0.03˚, and the elevation angle differences between the hyperbolic umbilicus fringes are 0.049˚ and 0.02˚.

4. Conclusion

When the ratio between the droplet equatorial radius and the Gaussian beam waist is the same, the influence of the droplet size change on the optical caustics is formed when the Gaussian beam is concentrically incident on the droplet. The curvature of the rainbow fringes and the position of the cusp caustics are calculated as the particle size increases. When the relative position of the Gaussian beam and the droplet changes, the optical caustics change accordingly. When γ (the drop/beam ratios) is the same, with the increase of the droplet size, the optical caustics formed by the Gaussian beam coaxially irradiating the ellipsoid droplets will gradually approach the optical caustics formed by the parallel beams. A method to measure the ellipsoid of droplets with different size ranges using Gaussian beams is proposed. When γ is the same, changing the distance d between the center of the Gaussian beam and the center of the ellipsoid droplet on the y-axis (within the Rayleigh length), or changing the distance d between the center of the Gaussian beam and the center of the ellipsoid droplet on the z-axis, the results show that with the increase of d, the optical caustics at this time will be the same as that of the Gaussian droplet. The optical caustics of the beam concentrically irradiating the droplet gradually move away, and this phenomenon will weaken as the droplet size increases. The above research results can be used to measure the aspect ratio of droplets with a wider range of particle sizes, and provide theoretical support for measuring droplet shape using Gaussian beams.

Conflicts of Interest

The author declares no conflicts of interest regarding the publication of this paper.

References

[1] Roth, N., Anders, K. and Frohn, A. (1990) Simultaneous Measurement of Temperature and Size of Droplets in the Micrometer Range. *Journal of Laser Application*, **2**, 37-42. https://doi.org/10.2351/1.4745251

[2] Marston, P.L. and Trinh, E.H. (1984) Hyperbolic Umbilic Diffraction Catastrophe and Rainbow Scattering from Spheroidal Drops. *Nature*, **312**, 529-531. https://doi.org/10.1038/312529a0

[3] Nye, J.F. (1984) Rainbow Scattering from Spheroidal Drops—An Explanation of the Hyperbolic Umbilic Foci. *Nature*, **312**, 531-532. https://doi.org/10.1038/312531a0

[4] Marston, P.L. (1985) Cusp Diffraction Catastrophe from Spheroids: Generalized

Rainbows and Inverse Scattering. *Optics Letters*, **10**, 588-590. https://doi.org/10.1364/OL.10.000588

[5] Marston, P.L. (1987) Transverse Cusp Diffraction Catastrophes: Some Pertinent Wave Fronts and a Pearcey Approximation to the Wave Field. *Journal of the Acoustical Society of America*, **81**, 226-232. https://doi.org/10.1121/1.394941

[6] Marston, P.L. (1999) Catastrophe Optics of Spheroidal Drops and Generalized Rainbows. *Journal of Quantitative Spectroscopy and Radiative Transfer*, **63**, 341-351. https://doi.org/10.1016/S0022-4073(99)00023-0

[7] Dean, C.E. and Marston, P.L. (1991) Opening Rate of the Transverse Cusp Diffraction Catastrophe in Light Scattered by Oblate Spheroidal Drops. *Applied Optics*, **30**, 3443-3451. https://doi.org/10.1364/AO.30.003443

[8] Nye, J.F. (1992) Rainbows from Ellipsoidal Water Drops. *Proceedings of the Royal Society of London Series A. Mathematical and Physical Sciences*, **438**, 397-417. https://doi.org/10.1098/rspa.1992.0115

[9] Simpson, H.J. and Marston, P.L. (1991) Scattering of White Light from Levitated Oblate Water Drops Near Rainbows and Other Diffraction Catastrophes. *Applied Optics*, **30**, 3468-3473. https://doi.org/10.1364/AO.30.003468

[10] Kaduchak, G., Marston, P.L. and Simpson, H.J. (1991) E_6 Diffraction Catastrophe of the Primary Rainbow of Oblate Water Drops: Observations with White-Light and Laser Illumination. *Applied Optics*, **33**, 4691-4696. https://doi.org/10.1364/AO.33.004691

[11] Kaduchak, G. and Marston, P.L. (1994) Hyperbolic Umbilic and E6 Diffraction Catastrophes Associated with the Secondary Rainbow of Oblate Water Drops: Observations with Laser Illumination. *Applied Optics*, **33**, 4697-4701. https://doi.org/10.1364/AO.33.004697

[12] Marston, P.L. and Kaduchak, G. (1994) Generalized Rainbows and Unfolded Glories of Oblate Drops: Organization for Multiple Internal Reflections and Extension of Cusps into Alexander's Dark Band. *Applied Optics*, **33**, 4702-4713. https://doi.org/10.1364/AO.33.004702

[13] Langley, D.S. and Marston, P.L. (1998) Generalized Tertiary Rainbow of Slightly Oblate Drops: Observations with Laser Illumination. *Applied Optics*, **37**, 1520-1526. https://doi.org/10.1364/AO.37.001520

[14] Lock, J.A. and Hovenac, E.A. (1991) Internal Caustic Structure of Illuminated Liquid Droplets. *Journal of the Optical Society of America A*, **8**, 1541-1552. https://doi.org/10.1364/JOSAA.8.001541

[15] Jobe, O., Thiessen, D.B. and Marston, P.L. (2017) Hyperbolic Umbilic Caustics from Oblate Water Drops with Tilted Illumination: Observations. *Journal of Quantitative Spectroscopy and Radiative Transfer*, **202**, 147-153. https://doi.org/10.1016/j.jqsrt.2017.07.036

[16] Roth, N., Anders, K. and Frohn, A. (1996) Size Insensitive Rainbow Refractometry: Theoretical Aspects. 8*th International Symposium on Applications of Laser Techniques to Fluid Mechanics*, Lisbon, 8-11 July 1996, 9.21-9.26.

[17] Van Beeck, J. and Riethmuller, M.L. (1995) Nonintrusive Measurements of Temperature and Size of Single Falling Raindrops. *Applied Optics*, **34**, 1633-1639. https://doi.org/10.1364/AO.34.001633

[18] Yu, H.T., Xu, F. and Tropea, C. (2013) Spheroidal Droplet Measurements Based on Generalized Rainbow Patterns. *Journal of Quantitative Spectroscopy & Radiative Transfer*, **126**, 105-112. https://doi.org/10.1016/j.jqsrt.2012.09.012

[19] van Beeck, J., Giannoulis, D., Zimmer, L. and Riethmuller, M.L. (1999) Global

Rainbow Thermometry for Droplet-Temperature Measurement. *Optics Letters*, **24**, 1696-1698. https://doi.org/10.1364/OL.24.001696

[20] van Beeck, J., Zimmer, L. and Riethmuller, M.L. (2001) Global Rainbow Thermometry for Mean Temperature and Size Measurement of Spray Droplets. *Particle & Particle Systems Characterization*, **18**, 196-204. https://doi.org/10.1002/1521-4117(200112)18:4<196::AID-PPSC196>3.0.CO;2-H

[21] Wu, Y.C., Promvongsa, J., Saengkaew, S., Wu, X., Chen, J. and Gréhan, G. (2016) Phase Rainbow Refractometry for Accurate Droplet Variation Characterization. *Optics Letters*, **41**, 4672-4675. https://doi.org/10.1364/OL.41.004672

[22] Wu, Y.C., Li, C., Cao, J.Z., Wu, X.C., Saengkaew, S., Chen, L.H., et al. (2018) Mixing Ratio Measurement in Multiple Sprays with Global Rainbow Refractometry. *Experimental Thermal & Fluid Science*, **98**, 309-316. https://doi.org/10.1016/j.expthermflusci.2018.06.004

[23] Yu, H.T, Shen, J.Q., Tropea, C. and Xu, F. (2019) Model for Computing Optical Caustic Partitions for the Primary Rainbow from Tilted Spheriodal Drops. *Optics Letter*s, **44**, 823-826. https://doi.org/10.1364/OL.44.000823

[24] Yu, H.T., Xu, F. and Tropea, C. (2013) Optical Caustics Associated with the Primary Rainbow of Oblate Droplets: Simulation and Application in Non-Sphericity Measurement. *Optics Express*, **21**, 25761-25771. https://doi.org/10.1364/OE.21.025761